Analyzing the effect of cell rearrangement on Delta-Notch pattern formation

Toshiki Oguma,[1] Hisako Takigawa-Imamura,[1] Tomoyasu Shinoda,[2] Shuntaro Ogura,[3] Akiyoshi Uemura,[3] Takaki Miyata,[2] Philip K. Maini,[4] and Takashi Miura[1]

[1]*Kyushu University Graduate School of Medical Sciences, Fukuoka 812-8582, Japan*

[2]*Nagoya University Graduate School of Medicine, Nagoya 466-8550, Japan*

[3]*Nagoya City University Graduate School of Medical Sciences, Nagoya 467-8601, Japan*

[4]*Wolfson Centre for Mathematical Biology, Mathematical Institute, Oxford OX2 6GG, United Kingdom*

(Received 29 June 2022; revised 22 March 2023; accepted 24 April 2023; published 14 June 2023)

The Delta-Notch system plays a vital role in many areas of biology and typically forms a salt and pepper pattern in which cells strongly expressing Delta and cells strongly expressing Notch are alternately aligned via lateral inhibition. In this study, we consider cell rearrangement events, such as cell mixing and proliferation, that alter the spatial structure itself and affect the pattern dynamics. We model cell rearrangement events by a Poisson process and analyze the model while preserving the discrete properties of the spatial structure. We investigate the effects of the intermittent perturbations arising from these cell rearrangement events on the discrete spatial structure itself in the context of pattern formation and by using an analytical approach, coupled with numerical simulation. We find that the homogeneous expression pattern is stabilized if the frequency of cell rearrangement events is sufficiently large. We analytically obtain the balanced frequencies of the cell rearrangement events where the decrease of the pattern amplitude, as a result of cell rearrangement, is balanced by the increase in amplitude due to the Delta-Notch interaction dynamics. Our framework, while applied here to the specific case of the Delta-Notch system, is applicable more widely to other pattern formation mechanisms.

DOI: 10.1103/PhysRevE.107.064404

I. INTRODUCTION

Discrete cell models can provide different pattern dynamics to those arising from continuous cell density models. Because living tissue is made up of cells, which act as the smallest discrete units in space, pattern formation on discrete spatial structures is observed in the context of biological pattern formation on a cellular scale. We study the effects of typical perturbations on the discrete spatial structure itself—flipping and duplication of the lattice—on pattern dynamics using analytical methods.

As an example of a mechanism that generates periodic pattern on a cellular scale, we will consider the Delta-Notch system. The Delta-Notch system is a well-studied cell-cell communication system and plays a critical role in many developmental processes [1–15]. Delta and Notch are, respectively, cell surface ligands and receptors. Delta expression in the neighborhood of a cell increases Notch expression in that cell which, in turn, decreases its Delta expression—a process known as "lateral inhibition." As a result, cells strongly expressing Delta and cells strongly expressing Notch are aligned alternately (the so-called "salt and pepper" pattern) [5].

Collier *et al.* [2] constructed the first mathematical model for the Delta-Notch system, which consisted of a spatially discrete ordinary differential equation system which was then analyzed, and necessary and sufficient conditions for a salt and pepper pattern were derived. To account for stochasticity in the cell-cell interactions and gene expression in signal transduction [16–18], a number of subsequent theoretical studies have incorporated stochasticity and revealed that, while low-intensity noise contributes to fine-grained pattern formation, high-intensity noise disrupts the salt and pepper pattern [16,19,20].

However, little research has been conducted to investigate the effect of positional perturbations arising from cell mixing and proliferation, despite these phenomena being generally observed [21–25]. Therefore, cell rearrangement by cell mixing and proliferation should significantly affect Delta-Notch pattern formation since the cells of interacting neighbors are changing. Germano *et al.* [26] have used a computational model to show that excessive cell turnover homogenizes Delta expression, while Stepanova *et al.* [27] developed a computational model to investigate how vascular structures are rearranged in response to the VEGF-Delta-Notch system. However, to analytically understand the effect of cell rearrangement on pattern formation, a simpler model is required.

In this study, we provide a framework to analytically evaluate the effect of stochastic and spatial perturbations arising from cell mixing and proliferation. We construct a simple stochastic differential equation model that incorporates Delta-Notch interaction and cell rearrangement events (cell mixing and proliferation) in one spatial dimension. Our numerical simulations show that the effect of cell rearrangement is to stabilize the homogeneous steady state and we provide a framework to analytically evaluate the stability of the pattern dynamics. Our analytical framework is consistent with numerical calculations and provides insight into how model parameters and frequencies of flipping or proliferation balance in the context of pattern formation.

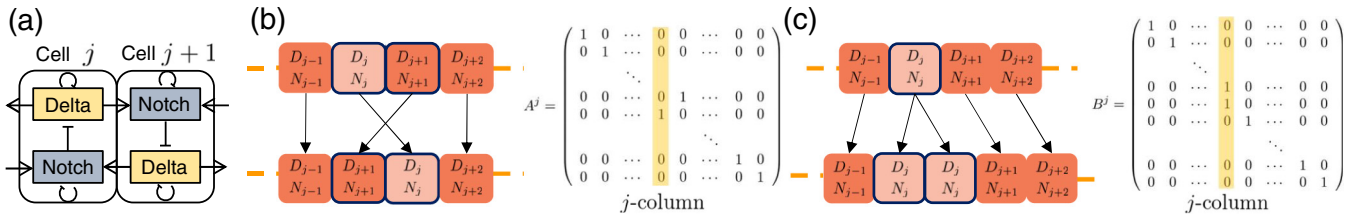

FIG. 1. (a) Schematic of the Delta-Notch interaction in the Collier model. Notch expression inhibits Delta expression, Delta expression promotes Notch expression in adjacent cells, and Delta and Notch themselves naturally decay. (b) Schematic of the flip event in the cell mixing model and the matrix A^j in (4). The flip event occurs according to the Poisson process with intensity p in each pair of cells. (c) Schematic of the duplication event in the cell proliferation model and the matrix B^j in (6). The duplication event occurs according to the Poisson process with intensity q in each cell.

II. METHODS AND MODELS

A. Numerical simulations

The numerical simulations were performed using MATHEMATICA (Wolfram) and JULIA (MIT) and we used periodic boundary conditions and an explicit Euler scheme.

For simulation of the Collier model (1), we used the following conditions, unless otherwise stated in the figure captions. Initial cell number $n = 100$, time step $\Delta t = 0.001$, duration $t = 1000$ (iteration 1 000 000), and parameter set $(v, \beta, h, r) = (1, 100, 4, 40)$. Initial conditions are $D_x(0) = D^0 + \kappa$ and $N_x(0) = N^0 + \kappa$ for cell x. Here D^0 and N^0 are the spatially homogeneous steady state values (Appendix A) and κ is an independent random variable from the uniform distribution in $[-0.0001, 0.0001]$.

To incorporate cell flipping and proliferation in the Delta-Notch model (1), we assumed that these events occur following a Poisson process with rates p and q, respectively.

B. Classical Delta-Notch model

To model the effect of cell mixing or proliferation on Delta-Notch pattern formation, we started with a version of the Collier model [2]. In this model, the Delta and Notch activities of a cell x (D_x and N_x, respectively) in a one-dimensional cell line were modeled [Fig. 1(a)] as below:

$$\frac{dD_x}{dt} = v\left(\frac{1}{1+\beta {N_x}^h} - D_x\right),$$
$$\frac{dN_x}{dt} = \frac{r\,(D_{x-1}+D_{x+1})}{1+r\,(D_{x-1}+D_{x+1})} - N_x. \qquad (1)$$

Here, the parameter v denotes the reaction speed of Delta dynamics relative to that of Notch. The parameters h and β denote the Hill coefficient and the intensity of Delta suppression by Notch, respectively. As the Delta activity in neighboring cells $(D_{x-1} + D_{x+1})$ increases, the activation of the Notch activity also increases, reaching a saturation level. The parameter r is a measure of the intensity of Notch activation by the Delta presented in neighboring cells. The number of cells is n and the position of the cell is x ($x \in \mathbb{N}$, $1 \leqslant x \leqslant n$).

We used a one-dimensional model because it is tractable analytically and the distinct salt and pepper pattern of Delta-Notch expression has been reported in endothelial cells which are aligned one dimensionally [8,13,14]. We assume that the number of cells is sufficiently large so that we can use periodic boundary conditions. This is because the effect of boundary conditions is confined near the boundary and the global pattern we focused on is minimally affected by the precise form of the boundary conditions if the system size is large. We confirmed, using numerical simulation, that the main results of this study are robust to different imposed boundary conditions (results not shown).

In the Collier model we use (1), whether or not a salt and pepper pattern emerges depends on the model parameters (v, β, h, r). The necessary and sufficient conditions for salt and pepper pattern formation are obtained by performing a standard linear stability analysis (Appendix A), requiring that the maximum eigenvalue be greater than zero:

$$\lambda_{\max} = \frac{-(a+d) + \sqrt{(a+d)^2 - 4(ad - 2b\alpha)}}{2} > 0, \qquad (2)$$

where $a = v$, $b = [\beta h v (N^0)^{h-1}]/[1 + \beta (N^0)^h]^2$, $d = 1$, $\alpha = r/[(1 + 2rD^0)^2]$, and (D^0, N^0) is the spatially homogeneous steady state of the Collier model (1). For example, the parameter β, which indicates the intensity of Delta suppression by Notch, broadens the region where $\lambda(\theta)$ is positive and increases $\lambda_{\max}$ (Appendix A and Fig. S1 [28]). Based on this analysis, we proceeded to investigate how pattern formation is altered by cell mixing and proliferation.

C. Cell mixing model

To introduce the effect of cell mixing on the Collier model (1), we modeled cell mixing as a series of flips between neighboring cells. We made several assumptions as follows [Fig. 1(b)].

(M1) The positions of the neighboring cells are randomly exchanged by cell flips in a single step.

(M2) Flips occur according to a Poisson process with intensity p in each pair of cells.

Let the vertical vectors $\boldsymbol{D}$ and $\boldsymbol{N}$, respectively, denote Delta and Notch expression in each cell as below:

$$\boldsymbol{D} = (D_1, D_2, \ldots, D_x, \ldots, D_n)^{\mathsf{T}},$$
$$\boldsymbol{N} = (N_1, N_2, \ldots, N_x, \ldots, N_n)^{\mathsf{T}}, \qquad (3)$$

and a flip between cells $x = j$ and $x = j + 1$ is described by multiplication with the $n \times n$ matrix A^j, which is generated by swapping the jth and $(j + 1)$th rows of the identity matrix as

below:

$$\{A^j\}_{k,m} = \begin{cases} 1 & \text{if } (k = m \text{ and } k \neq j, j+1) \\ & \text{or } (k = j \text{ and } m = j+1) \\ & \text{or } (k = j+1 \text{ and } m = j), \\ 0 & \text{otherwise,} \end{cases} \tag{4}$$

where $j+1$ is regarded as 1 if $j = n$ (periodic boundary condition). The effect of cell flipping was introduced by stochastically multiplying the matrix A^j by $\boldsymbol{D}$ and $\boldsymbol{N}$. Hence our cell mixing model is defined by the system of stochastic differential equations as below:

$$\begin{aligned} d\boldsymbol{D} &= \boldsymbol{f}(\boldsymbol{D}, \boldsymbol{N})dt + \sum_{j=1}^{n} (A^j - I)\, \boldsymbol{D}\, dL_t^{p,j}, \\ d\boldsymbol{N} &= \boldsymbol{g}(\boldsymbol{D}, \boldsymbol{N})dt + \sum_{j=1}^{n} (A^j - I)\, \boldsymbol{N}\, dL_t^{p,j}, \end{aligned} \tag{5}$$

where the functions $\boldsymbol{f}$ and $\boldsymbol{g}$ are the reaction terms of the Collier model (1), the matrix I denotes the identity matrix, and $L_t^{p,j}$ is the Poisson process with intensity p, which corresponds to the flip between cells j and $j+1$.

D. Cell proliferation model

To introduce the effect of cell proliferation on the Collier model (1), we modeled cell proliferation as the duplication of a cell. We also made several assumptions as follows [Fig. 1(c)].

(P1) The duplication process occurs in a single step.

(P2) The new cell is placed to the right of the original cell and inherits the same levels of Delta and Notch of the original cell.

(P3) The duplication process occurs according to the Poisson process with intensity q for each cell.

Assumptions (P2) and (P3) implicitly assume, respectively, that Delta and Notch activities are determined by their concentrations [29], and cell proliferation follows a memoryless stochastic process [30]. We denote Delta and Notch expression by the vertical vectors $\boldsymbol{D}_n = (D_1, D_2, \ldots, D_n)^{\mathsf{T}}$ and $\boldsymbol{N}_n = (N_1, N_2, \ldots, N_n)^{\mathsf{T}}$, respectively. Note that the number of cells (the dimension of the vectors $\boldsymbol{D}_n$ and $\boldsymbol{N}_n$) n increases with time. Under these assumptions, duplication of cell j is accounted for by defining the $(n+1) \times n$ matrix B^j, which is generated by duplicating the jth row of the identity matrix as below:

$$\{B^j\}_{k,m} = \begin{cases} 1 & \text{if } (k = m \text{ and } k \leqslant j) \\ & \text{or } (k = m+1 \text{ and } k \geqslant j), \\ 0 & \text{otherwise,} \end{cases} \tag{6}$$

and stochastically multiplying this matrix by $\boldsymbol{D}_n$ and $\boldsymbol{N}_n$, respectively:

$$\begin{aligned} &\text{if } dL_t^{q,j} = 0, \begin{cases} \boldsymbol{D}_n(t+dt) = \boldsymbol{D}_n(t) + \boldsymbol{f}(\boldsymbol{D}_n, \boldsymbol{N}_n)dt, \\ \boldsymbol{N}_n(t+dt) = \boldsymbol{N}_n(t) + \boldsymbol{g}(\boldsymbol{D}_n, \boldsymbol{N}_n)dt, \end{cases} \\ &\text{if } dL_t^{q,j} = 1, \begin{cases} \boldsymbol{D}_{n+1}(t+dt) = B^j[\boldsymbol{D}_n(t) + \boldsymbol{f}(\boldsymbol{D}_n, \boldsymbol{N}_n)dt], \\ \boldsymbol{N}_{n+1}(t+dt) = B^j[\boldsymbol{N}_n(t) + \boldsymbol{g}(\boldsymbol{D}_n, \boldsymbol{N}_n)dt]. \end{cases} \end{aligned} \tag{7}$$

Note that n will increase with time according to the Poisson process, so the size of B^j will also increase with time.

III. RESULTS

A. Numerical simulations with cell rearrangement

We set the parameters (v, β, h, r) such that linear analysis predicts the salt and pepper pattern when there is no cell rearrangement (without cell mixing or proliferation) and we simulated the model [Fig. 2(a)]. We then included cell rearrangement and found that the heterogeneity of the Delta-Notch pattern was decreased by cell rearrangement and the homogeneous steady state became stable again for a sufficiently high level of cell rearrangement [Figs. 2(b) and 2(c)]. More precisely, when the flip frequency $p = 0.001$, the salt and pepper pattern was largely maintained. However, for increasing values of p, the amplitude of the pattern became smaller. When p was sufficiently large, the amplitude was almost zero for the whole region and the system relaxed to the spatially homogeneous steady state [Fig. 2(b)]. In addition, as p increases, the expression pattern shows an envelope structure, in which the amplitude of the periodic pattern follows a longer pattern that oscillates. Similar results were obtained with the cell proliferation model [Fig. 2(c)]. With increasing proliferation frequency q, the amplitude of the pattern became smaller and, finally, the system settled back to a homogeneous steady state. These results are robust to 100 different runs of numerical simulations for each parameter set. Corresponding results are also obtained with different values of β and r (Fig. S2 and Fig. S3 [28]), suggesting that the stabilization of the homogeneous steady state by cell rearrangement events is a robust phenomenon.

To quantify the heterogeneity of the expression pattern, we introduce the heterogeneity function, $H(t)$, as the variance of the Delta expression:

$$H(t) = \frac{1}{n}\sum_{x=1}^{n}[D_x(t) - \langle D(t)\rangle]^2 = \frac{1}{n}\sum_{x=1}^{n}[D_x(t)^2 - \langle D(t)\rangle^2], \tag{8}$$

where

$$\langle D(t)\rangle = \frac{1}{n}\sum_{x=1}^{n} D_x(t). \tag{9}$$

If the salt and pepper pattern is completely formed, then $H(t)$ is close to the squared value of the amplitude of the pattern. If Delta expression is spatially homogeneous at the steady state, then $H(t) = 0$.

In both models, at the onset of the simulation, $H(t)$ decreases and then either increases or still decreases depending on the value of p in the cell mixing model or the value of q in the cell proliferation model (Figs. S4 and S5 [28]). This is because, at the onset, the initial random state is smoothened by the Delta-Notch dynamics. As we are interested in pattern growth after a sufficient time has elapsed, we define H_0 as the minimum heterogeneity in the time evolution of the no cell rearrangement model (Fig. S4 and Table S1 [28]):

$$H_0 = \min[H(t)]. \tag{10}$$

Then we define the normalized heterogeneity $H^*(t)$ as $H^*(t) = H(t)/H_0$, which is plotted in Fig. 3. Figure 3 shows

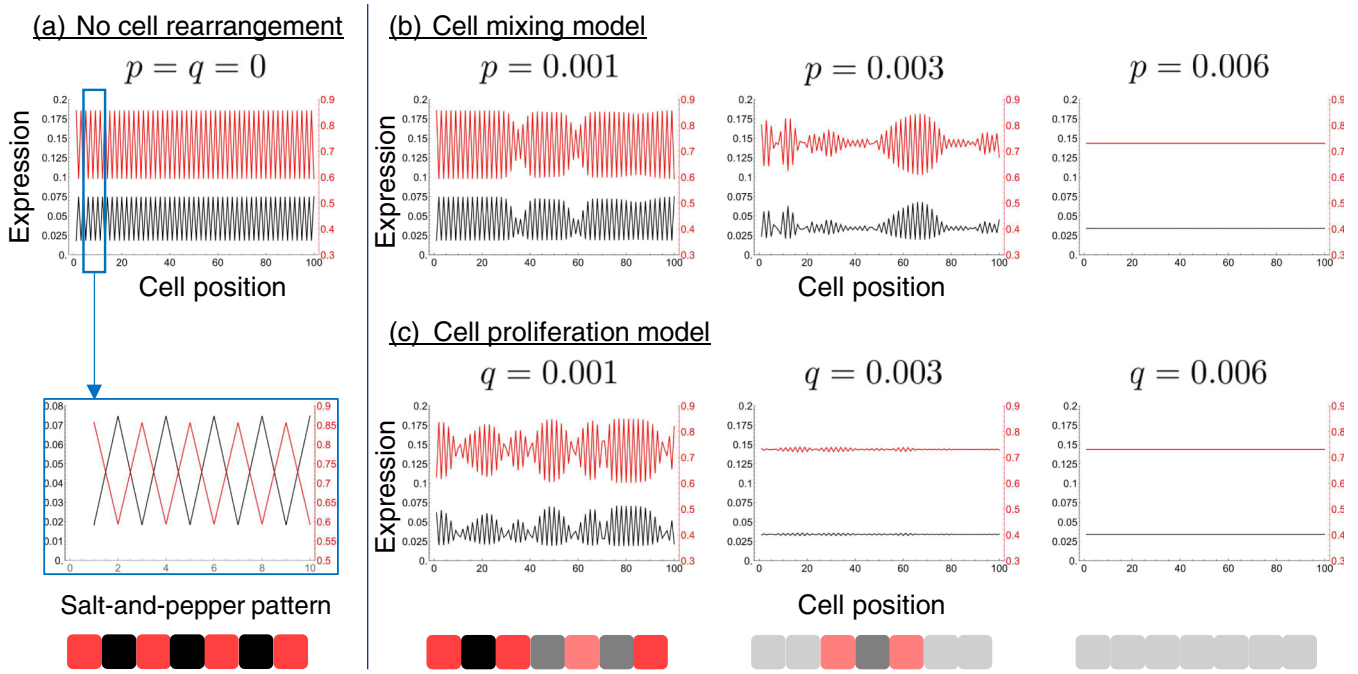

FIG. 2. Numerical simulations of the standard Delta-Notch model (1), the cell mixing model (5), and the cell proliferation model (7). (a) Standard model (no cell rearrangement). The red line represents Notch expression and the black line represents Delta expression. Delta and Notch are alternately expressed and the classical salt and pepper pattern emerges. (b) Cell mixing model (5). Numerical simulations are performed for different flipping frequencies $p = 0.001, 0.003, 0.006$. (c) Cell proliferation model (7). Numerical simulations are performed for different proliferation frequencies $q = 0.001, 0.003, 0.006$. The expression patterns of the first 100 cells are shown. Initial cell number $n = 100$, time step $\Delta t = 0.01$, duration $t = 1000$, and $(v, \beta, h, r) = (1, 100, 4, 40)$. Initial condition, $D_x(0) = D^0 + \kappa_x$ and $N_x(0) = N^0 + \kappa_x$, where D^0 and N^0 are the spatially homogeneous steady state values (Appendix A) and κ_x is a random variable from the uniform distribution in $[-0.02, 0.02]$.

that $H^*(t)$ switches between increasing and decreasing depending on the values of p and q. In the cell mixing model, it appears that $H^*(t)$ increases for $p \leqslant 0.005$ and decreases for $p > 0.005$ [Fig. 3(a) and Fig. S5(A) [28]]. In the cell proliferation model, $H^*(t)$ increases for $q \leqslant 0.0045$ and decreases for $q > 0.0045$ [Fig. 3(b) and Fig. S5(B) [28]]. These results suggest that there exist balanced frequencies p^* and q^* for which the attenuation of the pattern by cell rearrangement and its formation by the Delta-Notch dynamics are balanced.

We numerically estimated the balanced frequencies and the growth rate of the heterogeneity. For the balanced frequencies p^* and q^*, we estimated the intersection points of the plot of $\ln H^*(t)$ as a function of p and q and the plot of $\ln H^*(t) = 0$. We performed linear regression for the data points whose value of $\log_{10} H^* \in [-8, 4]$ in Fig. 3 and estimated p^* and q^* as the intersection points of the fitted lines and the function $\ln H^*(t) = 0$ [Figs. 4(c) and 4(f), black dots]. For the growth rate of the heterogeneity, we estimated the slope of the line that was fitted to the plot of $\ln H^*(t)$ against t. Similarly, we performed linear regression for the data points in the range $\log_{10} H^* \in [-8, 4]$ in Fig. S7 [28] and estimated y and j as the slopes of the fitted lines [Figs. 4(a) and 4(d), black dots].

B. Analysis of the cell rearrangement models

To quantify the effects of cell rearrangement (mixing and proliferation), we analyzed the stability of the pattern dynamics and the balanced frequencies p^* and q^*. The "tug of war" of the cell rearrangement and the Delta-Notch dynamics was represented as the growth or attenuation of the heterogeneity $H(t)$. Therefore, we focused on the effect of cell rearrangement on $H(t)$.

The heterogeneity $H(t)$ can also be calculated from the power spectrum of the Delta expression pattern. The power spectrum P_k of the Delta expression pattern is the squared absolute value of the Fourier coefficient δ_k of Delta expression (Appendix A), so P_k can be calculated as

$$P_k(t) = |\delta_k(t)|^2 = \left| \frac{1}{n} \sum_{x=1}^{n} D_x(t) e^{\frac{-i2\pi kx}{n}} \right|^2. \tag{11}$$

Note that k takes integer values from 0 to $n-1$ and n increases with time in the cell proliferation model. From Parseval's theorem,

$$\sum_{x=1}^{n} D_x(t)^2 = \sum_{k=0}^{n-1} P_k(t), \tag{12}$$

and, from (11),

$$\langle D_x(t) \rangle^2 = \left(\frac{1}{n} \sum_{x=1}^{n} D_x(t) \right)^2 = P_0(t). \tag{13}$$

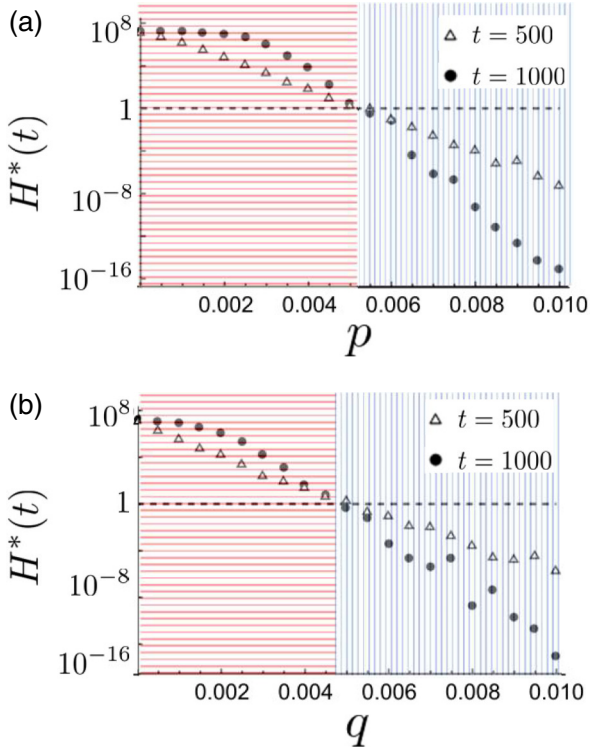

FIG. 3. Log plots of the normalized heterogeneity of the pattern $H^*(t)$ against the frequencies of the cell rearrangement events for $t = 500$ and 1000. The black dashed line represents the plot of $H^*(t) = 1$ and the circles and triangles represent $H^*(1000)$ and $H^*(500)$, respectively. (a) In the cell mixing model, $H^*(1000) > H^*(500) > 1$ with $p \leqslant 0.005$ (red horizontal stripe region) and $H^*(1000) < H^*(500) < 1$ with $p > 0.005$ (blue vertical stripe region). (b) In the cell proliferation model, similar inequalities hold and the threshold value is $q = 0.0045$. We calculated the heterogeneity at 21 different frequencies of p and q, which are taken in the range 0 to 0.01 at equal intervals of 0.0005 in each model. The heterogeneity $H^*(t)$ shown in this figure was calculated by taking the average of $H(t)$ over 400 different simulation runs, and then normalized by H_0, for each p and q. Other conditions are as in Fig. 2. Initial conditions are randomly determined from the same distribution as in Fig. 2 for each of the runs.

By substituting (12) and (13) into (8), $H(t)$ was calculated as below:

$$H(t) = \frac{1}{n}\sum_{k=1}^{n-1} P_k(t). \tag{14}$$

Therefore, $H(t)$ is proportional to the sum of squares of the amplitudes of all wavenumber components in the pattern.

The balanced frequencies p^* and q^* are independent of the definition of the heterogeneity $H(t)$. If we adopted the variance of the Notch expression instead of the Delta expression, then the dispersion relation and the effect of the cell rearrangement events A^j and B^j are the same as for the Delta expression and we obtained the same p^* and q^* as before. In addition, we can obtain the same p^* and q^* values if we defined the heterogeneity by the average of the squared values. For example, if we adopt $[\Sigma(D_x - D_{x+1})^2]/n$ as the heterogeneity, then we obtain the same p^* and q^* since this value is also calculated from the linear summation of the power spectrum (Fig. S6 [28]). We now proceed to analyze the stability of the power spectrum $P_k(t)$ in the cell mixing and proliferation models.

1. Cell mixing model

First, we will transform the cell mixing model (5) into the corresponding system of stochastic differential equations that represent the time evolution of the Fourier coefficients δ_k. To find the balanced frequency p^* and the onset of pattern formation, we assume that $H(t)$ is small since we set the initial condition to be a small perturbation about the homogeneous steady state, so the reaction terms $\boldsymbol{f}(\cdot)$ and $\boldsymbol{g}(\cdot)$ can be regarded as linear operators since $D_x \sim D^0$ and $N_x \sim N^0$. Therefore, the effect of the Delta-Notch dynamics on the Fourier coefficients δ_k of D_x is described by the diagonal matrix Λ from the linear stability analysis (Appendix A) as below:

$$\Lambda = \mathrm{diag}(\lambda_0, \lambda_1, \ldots, \lambda_{n-1}), \tag{15}$$

where

$$\lambda_k = \frac{-(a+d) + \sqrt{(a+d)^2 - 4[ad + 2b\alpha\,\cos(2\pi k/n)]}}{2}. \tag{16}$$

The effect on the Fourier coefficients δ_k of a cell flip is given by the $n \times n$ matrix C^j:

$$C^j = FA^jF^{-1}, \tag{17}$$

where F is the discrete Fourier transform matrix. The components of the matrices F and F^{-1} are given as below:

$$\{F\}_{l,m} = \frac{1}{\sqrt{n}} e^{-i2\pi(l-1)(m-1)/n}, \tag{18}$$

$$\{F^{-1}\}_{l,m} = \frac{1}{\sqrt{n}} e^{i2\pi(l-1)(m-1)/n}. \tag{19}$$

Therefore, the time evolution of the Fourier coefficients $\boldsymbol{\delta}$ can be described by

$$d\boldsymbol{\delta} = \Lambda\boldsymbol{\delta}\,dt + \sum_{j=1}^{n}(C^j - I)\boldsymbol{\delta}\,dL_t^{p,j}, \tag{20}$$

where $\boldsymbol{\delta} = [\delta_0(t), \delta_1(t), \ldots, \delta_k(t), \ldots, \delta_{n-1}(t)]^\mathsf{T}$.

Furthermore, we obtain the expected time evolution of the power spectrum by calculating the average of the effect of the cell flip on the power spectrum for j (Appendix B) as below:

$$d\boldsymbol{P} = 2\,\mathrm{Re}[\Lambda]\boldsymbol{P}\,dt + W\boldsymbol{P}\,dL_t^{pn}. \tag{21}$$

Here $\boldsymbol{P} = [P_0(t), P_1(t), \ldots, P_k(t), \ldots, P_{n-1}(t)]^\mathsf{T}$, L_t^{pn} is the Poisson process with intensity pn, and the components of the matrix W are given as below:

$$\{W\}_{l,m} = \begin{cases} -\frac{8}{n}\sin^2\frac{\pi(l-1)}{n} + \left(\frac{4}{n}\sin^2\frac{\pi(l-1)}{n}\right)^2 & (l = m), \\ \left(\frac{4}{n}\sin\frac{\pi(l-1)}{n}\sin\frac{\pi(m-1)}{n}\right)^2 & (\text{otherwise}). \end{cases} \tag{22}$$

Both the average and variance of the Poisson process L_t^{pn} are pnt, so those of L_t^{pn}/n are pt and pt/n, respectively. Therefore, when n is sufficiently large, dL_t^{pn}/n can be approximated

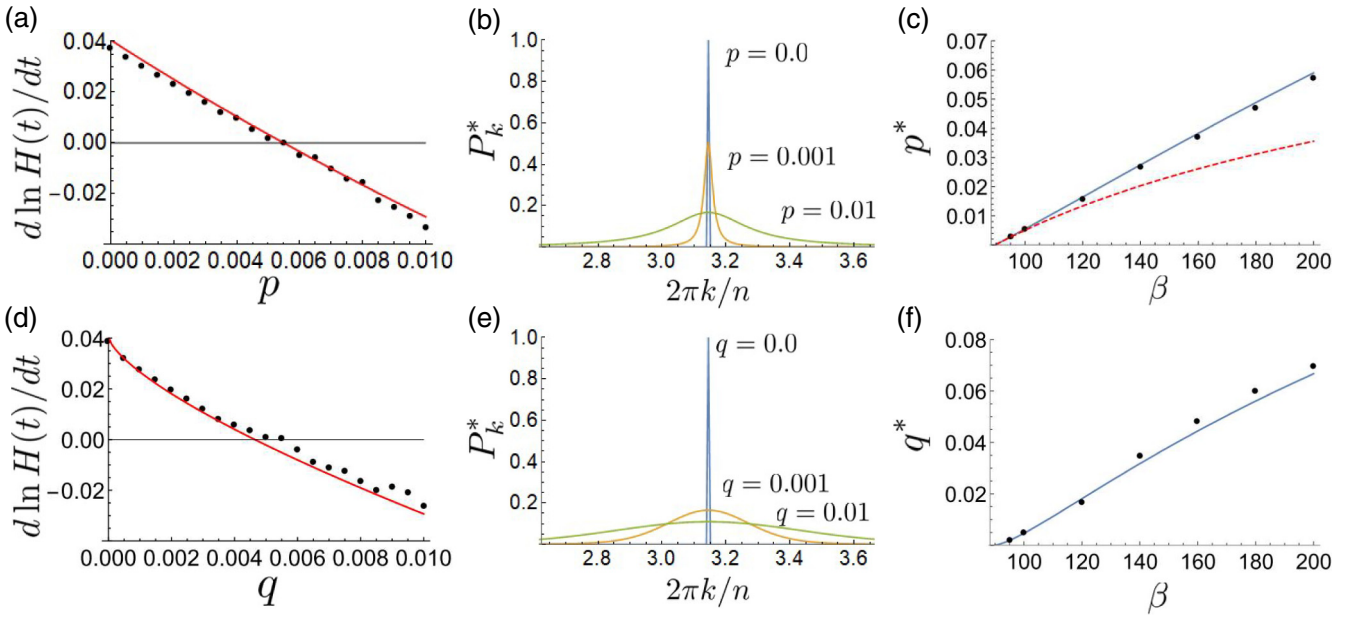

FIG. 4. Comparison between the analytical and numerical results. (a) The red line and the black dots represent the maximum eigenvalue y of the matrix Y_p in (23) and the growth rate $d \ln H(t)/dt$ estimated from Fig. S5(A) [28], respectively. (b) Components P_k^* of the corresponding eigenvector P^* normalized with the maximum eigenvalue of the matrix Y_p with $n = 1000$. (c) Balanced frequencies p^* plotted against the parameter β in the Collier model (1). The blue solid line represents the values of p such that the maximum eigenvalue of Y_p in (23) is zero, the red dashed line represents p^* derived from (29), and the black dots represent the values of p^* that were estimated from Fig. 3(a). (d) The red line and the black dots represent the maximum eigenvalue of the matrix J_q in (39) and the growth rate $d \ln H(t)/dt$ estimated from Fig. S5(B) [28], respectively. (e) Components P_k^* of the corresponding eigenvector $\boldsymbol{P^*}_n$ normalized with the maximum eigenvalue of the matrix J_q with $n = 1000$. (f) Balanced frequencies q^* plotted against the parameter β. The blue line represents the value of q such that the maximum eigenvalue of J_q in (39) is zero and the black dots represent the values of q^* that were estimated from Fig. 3(b), respectively. The numerically estimated growth rate $d \ln H(t)/dt$ [black dots in (a) and (d)] was calculated from the slope of the lines that were fitted to the plot of $\ln H(t)$ against t (Fig. S5 [28]). The numerically estimated balanced frequencies [black dots in (c) and (f)] were estimated as the intersection points of the plot of $\ln H^*(t)$ as a function of p and q and the plot of $\ln H^*(t) = 0$ in Fig. 3, respectively.

by pdt and Eq. (21) is approximated by

$$\frac{d}{dt}\boldsymbol{P} \simeq Y_p \boldsymbol{P}, \tag{23}$$

where

$$Y_p = 2\,\mathrm{Re}[\Lambda] + pnW. \tag{24}$$

Therefore, by using the maximum eigenvalue and the corresponding eigenvector of the matrix Y_p, we can derive the expected pattern dynamics.

If y is the maximum eigenvalue of Y_p and $\boldsymbol{P^*} = (P_0^*, P_1^*, \ldots, P_{n-1}^*)^\mathsf{T}$ is the corresponding eigenvector, then $\boldsymbol{P} \sim e^{yt}\boldsymbol{P^*}$ for values of t in a range sufficiently large so that other eigenvectors no longer affect the power spectrum, but not so large for nonlinear effects to come into play. The scaling law $H(t) \sim e^{yt}$ also holds, since $H(t)$ is a linear summation of the power spectrum $P_k(t)$. Therefore, the maximum eigenvalue y corresponds to the growth rate of the heterogeneity $d \ln H(t)/dt$. Figure 4(a) shows that the value of y derived from Eq. (23) agrees with the numerically estimated growth rate $d \ln H(t)/dt$ and Fig. 4(b) shows how the shape of the corresponding eigenvector $\boldsymbol{P^*}$ depends on p. Note that the effect of the Delta-Notch interaction $2\,\mathrm{Re}[\Lambda]$ on P_k is determined by the value of $2\pi k/n$, so we plot P_k^* against $2\pi k/n$ in Fig. 4(b).

To obtain the balanced frequency p^*, we used Newton's method to derive the value of p such that the maximum eigenvalue of Y_p is zero. The values of p^* obtained in this way are in very good agreement with the corresponding values estimated from the numerical simulations of (5) for varying β [Figs. 4(c) and S7 [28]] and r (Fig. S8 [28]). In addition, the values of y and p^* obtained in Figs. 4(a) and 4(c) are almost identical for $n \geqslant 100$ [Figs. S9(A) and S9(B) [28]].

Furthermore, we obtain the growth rate $d \ln H(t)/dt$ and the balanced frequency p^* as $n \to \infty$ as solutions of the integral equations (Supplemental text A [28]). They are also in very good agreement with the numerically estimated values.

We can derive an approximation to the balanced frequency p^* from the linear stability analysis of the spatially uniform steady state in the deterministic system that is obtained by regarding the effect of cell mixing as a diffusion process:

$$\begin{aligned}\frac{dD_x}{dt} &= v\left(\frac{1}{1+\beta {N_x}^h} - D_x\right) + p(D_{x-1} + D_{x+1} - 2D_x),\\ \frac{dN_x}{dt} &= \frac{r(D_{x-1} + D_{x+1})}{1 + r(D_{x-1} + D_{x+1})} - N_x + p(N_{x-1} + N_{x+1} - 2N_x).\end{aligned} \tag{25}$$

System (25) has the same spatially homogeneous steady state as in (1), so we can linearize the system as in Appendix A and

obtain the Jacobian matrix:

$$\tilde{M}_k = \begin{pmatrix} -a - 4p\,\sin^2(\pi k/n) & -b \\ 2\alpha\,\cos(2\pi k/n) & -d - 4p\,\sin^2(\pi k/n) \end{pmatrix}. \tag{26}$$

The eigenvalue $\tilde{\lambda}_k$ with the larger real part, obtained from the matrix $\tilde{M}_k$, is

$$\tilde{\lambda}_k = \lambda_k - 4p\,\sin^2\frac{\pi k}{n}, \tag{27}$$

where λ_k is given by (A9), so the time evolution of the power spectrum can be approximated by

$$\frac{d}{dt}P_k = \left(2\,\mathrm{Re}[\lambda_k] - 8p\,\sin^2\frac{\pi k}{n}\right)P_k. \tag{28}$$

This equation corresponds to the system that is obtained by ignoring the nondiagonal components of the matrix Y_p in (23). From (28), the balanced frequency p^* is approximated as p such that

$$\max_{\theta\in[0,2\pi)}\left[\mathrm{Re}[\lambda(\theta)] - 4p\,\sin^2\frac{\theta}{2}\right] = 0. \tag{29}$$

When the range of θ for which $\lambda(\theta)$ is positive is sufficiently narrow, the values of P_k, except around $k = n/2$, quickly decay. Hence the nondiagonal components of the matrix Y_p are ignorable and we can approximate the effect of cell mixing as a diffusion of the Delta and Notch activities.

Figure 4(c) shows that the estimation in Eq. (29) is a good approximation for $95 < \beta < 120$. If $\lambda(\theta)$ is positive only in the region that is very close to $\theta = \pi$, then we can obtain the simpler form of (29):

$$p^* = \lambda_{\max}/4. \tag{30}$$

Here $\lambda_{\max}$ is given by Eq. (2) and we used the approximation $\sin^2(\theta/2) \simeq 1$ in the region that is close to $\theta = \pi$. Consistent with (30), $\lambda_{\max}$ was 0.02 and the balanced frequency p^* was estimated around 0.005 for the conditions used in Fig. 3.

2. Cell proliferation model

The cell proliferation model (7) was also analytically transformed into the corresponding system of stochastic differential equations that represent the time evolution of δ_k. The effect of a cell proliferation event, which increases the cell number n to $n+1$, on the Fourier coefficients $\boldsymbol{\delta}_n$, is given as below:

$$\hat{C}^j = \hat{F}B_jF^{-1}, \tag{31}$$

where $\hat{F}$ is a square $(n+1)\times(n+1)$ matrix, F^{-1} is the square $(n\times n)$ matrix defined in (19), and B_j is the $(n+1)\times n$ matrix given by (6). The matrix $\hat{F}$ is defined by

$$\{\hat{F}\}_{l,m} = \frac{1}{\sqrt{n+1}}e^{-i2\pi(l-1)(m-1)/(n+1)}. \tag{32}$$

Therefore, the time evolution of $\boldsymbol{\delta}_n(t)$ is given as below:

$$\begin{aligned} \boldsymbol{\delta}_n(t+dt) &= e^{\Lambda\,dt}\boldsymbol{\delta}_n(t) \quad \text{if } dL_t^{q,j} = 0, \\ \boldsymbol{\delta}_{n+1}(t+dt) &= \hat{C}^j e^{\Lambda\,dt}\boldsymbol{\delta}_n(t) \quad \text{if } dL_t^{q,j} = 1. \end{aligned} \tag{33}$$

By calculating the average of the effect of the cell proliferation event for j, the expected time evolution of the power spectrum $\boldsymbol{P}_n(t)$ is given (Appendix C) by

$$\begin{aligned} \boldsymbol{P}_n(t+dt) &= e^{2\,\mathrm{Re}[\Lambda]dt}\boldsymbol{P}_n(t) \quad \text{if } dL_t^{qn} = 0, \\ \boldsymbol{P}_{n+1}(t+dt) &= S\,e^{2\,\mathrm{Re}[\Lambda]dt}\boldsymbol{P}_n(t) \quad \text{if } dL_t^{qn} = 1, \end{aligned} \tag{34}$$

where the components of the matrix S are given by

$$\{S\}_{l,m} = \begin{cases} (n+1)/n & (\text{if } l = m = 1), \\ \frac{1}{n(n+1)}\frac{\sin^2\frac{\pi m}{n}}{\sin^2(\frac{\pi l}{n+1}-\frac{\pi m}{n})} & (\text{otherwise}). \end{cases} \tag{35}$$

Since the matrix S is nonsquare, the stability of the homogeneous steady state cannot be determined as in the cell mixing model. Hence we approximate the matrix S by a square matrix, as below.

The power spectrum $\boldsymbol{P}_n$ is represented by the superposition of the cosine waves from the symmetry $P_k = P_{n-k}$. By assuming that the shortest wavelength component of $S\boldsymbol{P}_n$ is negligible, the matrix S is approximated by the square matrix Σ (given below) and Eq. (34) is approximated by (Appendix C)

$$d\boldsymbol{P}_n \simeq 2\,\mathrm{Re}[\Lambda]\boldsymbol{P}_n dt + (\Sigma - I)\boldsymbol{P}_n dL_t^{qn}, \tag{36}$$

where I is the identity matrix. When n is even, the components of the matrix Σ are given by

$$\begin{aligned} \{\Sigma\}_{l,m} =& \frac{2}{n}\sum_{k=2}^{n/2}\cos\frac{2\pi(m-1)(k-1)}{n}\left[\frac{k-1}{n+1}\cos\frac{2\pi(l-1)(k-2)}{n} + \left(1-\frac{k-1}{n+1}\right)\cos\frac{2\pi(l-1)(k-1)}{n}\right] \\ &+ \frac{1}{n}\left[1 + (-1)^{m+k-2}\left(1 - \frac{n}{n+1}\sin^2\frac{\pi(m-1)}{n}\right)\right] \end{aligned} \tag{37}$$

and when n is odd

$$\{\Sigma\}_{l,m} = \frac{2}{n}\sum_{k=2}^{(n+1)/2}\cos\frac{2\pi(m-1)(k-1)}{n}\left[\frac{k-1}{n+1}\cos\frac{2\pi(l-1)(k-2)}{n} + \left(1-\frac{k-1}{n+1}\right)\cos\frac{2\pi(l-1)(k-1)}{n}\right] + \frac{1}{n}. \tag{38}$$

As in the cell mixing model, assuming n is sufficiently large, L_t^{qn}/n is approximated by qt as in the cell mixing model, so the time evolution of $\boldsymbol{P}_n$ in (36) is approximated by

$$\frac{d}{dt}\boldsymbol{P}_n \simeq J_q\boldsymbol{P}_n, \tag{39}$$

where

$$J_q = 2\,\mathrm{Re}[\Lambda] + qn(\Sigma - I). \tag{40}$$

Therefore, by using the maximum eigenvalue and the corresponding eigenvector of the matrix J_q, we can approximately derive the expected pattern dynamics.

Figure 4(d) shows that the maximum eigenvalue of the matrix J_q is in very good agreement with the numerically estimated growth rate $d \ln H(t)/dt$ and Fig. 4(e) shows how the shape of the corresponding eigenvector $\boldsymbol{P^*}_n$ depends on q.

To obtain the balanced frequency q^*, we used Newton's method to derive the value of q such that the maximum eigenvalue of J_q is zero. Figure 4(f) shows that the values of q^* obtained in this way are in very good agreement with the numerically estimated q^*. The values obtained in Figs. 4(d) and 4(f) are almost identical for $n \geqslant 100$ (Fig. S9 [28]), although the definition of the matrix Σ is different depending on whether n is odd or even.

3. Eigenvalue problems corresponding to (23) and (39) explain the pattern dynamics

In the above analysis, we have shown that the pattern dynamics of the cell mixing model and the cell proliferation model can be captured by solving for the maximum eigenvalue problem of the matrices Y_p (24) and J_q (40), respectively, and yield results that agree well with our numerical simulations of the full model.

First, the maximum eigenvalues of Y_p and J_q capture the growth or attenuation rate of the heterogeneity of the pattern. Figures 4(a) and 4(d) show that the exponents are consistent with the maximum eigenvalue y and j, respectively. Therefore, the balanced frequencies p^* and q^* are derived as the frequencies that make $y = 0$ and $j = 0$, respectively [Figs. 4(c), 4(f), and Fig. S8].

Second, the maximum eigenvalues y and j also explain the time for the pattern to be established. Figures S10(A) and (C) [28] show that the time required for $H(t)$ to reach a saturated value extends as p and q increase. Here, we define the characteristic time t^* as the time required for $H^*(t)$ to reach $H^*(10000)/e$ and find that the values of yt^* and jt^* for each p and q are within an error margin of 8.2% and 7.3%, respectively [Figs. S10(B) and S10(D) [28]]. Therefore, cell mixing and cell proliferation extend the time required for pattern establishment, as $t^* \sim 1/y$ and $t^* \sim 1/j$, respectively.

In addition, the eigenvectors corresponding to y and j, shown in Figs. 4(b) and 4(e), explain the pattern envelope in Fig. 2. Figure 4 shows that, in the model that includes only the Delta-Notch interaction, the eigenvector corresponding to the maximum eigenvalue has nonzero component only for $k = n/2$. On the other hand, in the model that includes cell mixing and proliferation, the eigenvector takes nonzero values for several wave numbers. When several wavelength components are mixed at a similar scale, the corresponding envelope pattern structure is generated.

Although cell mixing and proliferation similarly affect the pattern dynamics as discussed above, their individual effects on the power spectrum are qualitatively different. We performed numerical simulations of the model including only one of the processes (cell mixing, cell proliferation), without the Delta-Notch interaction and setting the salt and pepper pattern as the initial state. The results show that cell mixing, unsurprisingly, "scrambles" the pattern and the power spectrum is uniformly distributed, while cell proliferation elongates the periodic length of the pattern and shifts the power spectrum to the long-wavelength region (Fig. S11 [28]). This is because both effects are regarded as the redistribution of the power spectrum in frequency space since the determinants of W and Σ in Eqs. (22), and (37) and (38), respectively, are 1. Their eigenvectors, corresponding to the maximum eigenvalues, are shown in Fig. S11(E) [28]. The components of the eigenvector of W are all equal to each other and those of Σ have only one nonzero component for $k = 0$. These results mean that cell mixing smoothens the power spectrum so that it becomes uniformly distributed, while cell proliferation shifts the distribution of the power spectrum to the long-wavelength region. These differences correspond, in the absence of cell-cell interaction, to the scrambling of existing patterns due to cell mixing and elongation of an existing pattern due to cell proliferation. However, when they are incorporated into the Delta-Notch model, the pattern dynamics are dominated by the interaction between the increasing power spectrum around $k = n/2$ by Delta-Notch interaction and its redistribution by cell rearrangement. The pattern dynamics in the cell mixing and proliferation models become similar.

Based on the above discussion, the pattern dynamics of the Delta-Notch interaction with cell rearrangement events results in the growth and redistribution of the power spectrum. In the model that includes only Delta-Notch interaction, the power spectrum around $k = n/2$ grows according to the dispersion relation, while the rest of the spectrum decays (Appendix A). As a result, the power spectrum finally concentrates around $k = n/2$, which corresponds to the salt and pepper pattern. However, when cell mixing and proliferation are introduced, the power spectrum around $k = n/2$ is distributed to other regions and undergoes attenuation. If the attenuation of the redistributed power spectrum exceeds the growth of the power spectrum around $k = n/2$, then the sum of the power spectrum decreases, which means that the homogeneous steady state is stabilized. The cell flip and proliferation frequency at the balanced point is the balanced frequency p^* and q^*, respectively. Note that cell mixing and proliferation themselves do not stabilize the homogeneous steady state, but require the attenuation of the redistributed power spectrum due to the Delta-Notch interaction. Therefore, if the Delta and Notch activities are bistable without spatial interactions, as reported by Formosa-Jordan *et al.* [31], then the redistributed power spectrum is not attenuated. Hence the pattern is not homogenized, only disturbed.

IV. DISCUSSION

This paper provides a framework to analytically evaluate the effect on Delta-Notch pattern formation of cell rearrangement arising from migration or proliferation in a one-dimensional line of cells. We model cell rearrangement events as occurring intermittently and randomly in a discrete spatial linear structure. We modeled the intermittency of cell rearrangement events by a jump process and analyzed the model while maintaining the discreteness of the spatial

structure by considering the time evolution of the power spectrum. In our framework, the stochastic and intermittent effects of cell rearrangement were approximated by the deterministic effects on the power spectrum. Accordingly, the instabilities of the pattern dynamics were analyzed by solving the maximum eigenvalue problem of the resultant systems (23) and (39).

In endothelial cells within the retinal vasculature, the cells align in a one-dimensional array and Delta-Notch pattern formation [8,13,14], cell mixing and proliferation [23,24,32] occur. The expression pattern of Delta-like ligand 4 (Dll4) mRNA is alternating in arteries, and homogeneous in veins [Fig. S12(A)] [8,13,14]. Our preliminary experiments indicated that endothelial cell motility and proliferation rates are higher in veins than in arteries (Supplemental text B and Fig. S12 [28]). This relationship has also been reported in the developing zebrafish vasculature [33,34]. Our theoretical predictions regarding the relationship between the frequency of cell rearrangement events and expression patterns are consistent with these experimental findings.

In this study, we assumed that the daughter cells inherit the same activity of Delta and Notch in the cell proliferation model. However, if we adopt an asymmetric inheritance rule, we obtain different pattern dynamics. Figure S13 [28] shows how the magnitude of the perturbation to the expression in daughter cells caused by asymmetric cell division affects heterogeneity in the cell proliferation model (7). Although the steady value of $H(t)$ decreases with q as in the symmetric inheritance rule case, the time required to establish the pattern decreases and the pattern maintains a certain degree of heterogeneity even for large q and does not converge to the homogeneous steady state [Figs. S13(B) and S13(C)]. It should be noted, however, that the results exhibited for the symmetric inheritance rule are similar to those for the asymmetric inheritance rule, for small perturbations [Fig. S13(D)].

Our analysis can be applied to a wide range of pattern formation mechanisms. For example, a Delta-Notch interaction model that includes cis-interaction, which is the inhibition of Notch activity by Delta activity, is proposed by Sprinzak *et al.* [3]. This model (S47) consists of three variables and has different interaction terms when compared to the Collier model (1). We find that cell rearrangement events also inhibit salt and pepper pattern formation in the Sprinzak model and our analysis yields expressions for the balanced frequencies p^* and q^* that are consistent with the numerical results (Supplemental text E and Fig. S14 [28]). To determine the stability of the homogeneous steady state, our method is effective regardless of the details of the model, such as the number of variables and the interaction terms, and could be applied to models which include the effect of other ligands in the Delta-Notch system, such as the Delta-Notch-Jagged system [35].

In addition, phase synchronization phenomena in coupled agent-based models can be investigated by our analysis. Uriu *et al.* [36] showed that the exchange of positions in a coupled phase oscillator system in a one-dimensional array promoted phase synchronization and the relaxation time is consistent with the mean-field approximation if the exchange frequency is sufficiently large. This phase synchronization model is similar to the model we used, in the sense that interactions between neighboring cells are affected by positional perturbations, suggesting we can also capture this phenomenon by interpreting phase synchronization as convergence to a homogeneous steady state of the pattern composed of the agents' phase state. Replacing the effects of flip and proliferation by a linear operator acting on the power spectrum should be applicable to the other system of cell-cell interaction. (See also Refs. [37–43] for supplemental texts A–E.)

ACKNOWLEDGMENTS

The authors thank Prof. K. Nishiyama (Kumamoto University), Prof. S.-I. Ei (Hokkaido University), Dr. Y. Tanaka (Future University Hakodate), and Dr. K. Sugihara (Kyushu University) for helpful discussions. This work has been financially supported by JST CREST (Grant No. JPMJCR14W4 to T.M.), JSPS KAKENHI (Grant No. JP18K06260 to H.T.-I.), and TOBITATE! Study Abroad Initiative and Young Ambassador Program (to T.O.).

APPENDIX A: DISPERSION RELATION OF THE COLLIER MODEL

To derive the necessary and sufficient conditions for pattern formation, we performed a linear stability analysis of the Collier model (1).

The homogeneous steady state (D^0, N^0) in the Collier model (1) with periodic boundary conditions is given by

$$D^0 = \frac{1}{1+\beta(N^0)^h}, \tag{A1}$$

$$N^0 = \frac{2rD^0}{1+2rD^0}. \tag{A2}$$

By setting $D_x = D^0 + d_x, N_x = N^0 + n_x$, where $|d_x| \ll 1, |n_x| \ll 1$, the Collier model (1) can be linearized to obtain

$$\begin{aligned} \frac{d}{dt}d_x &= -ad_x - bn_x, \\ \frac{d}{dt}n_x &= -dn_x + \alpha(d_{x-1} + d_{x+1}), \end{aligned} \tag{A3}$$

where $a = v$, $b = [\beta h v (N^0)^{h-1}]/[1+\beta(N^0)^h]^2$, $d = 1$, and $\alpha = r/(1+2rD^0)^2$.

To examine the stability of the homogeneous steady state in the Collier model (1), we consider a discrete Fourier transformation of d_x, n_x as below:

$$\begin{aligned} \delta_k(t) &= \frac{1}{\sqrt{n}}\sum_{x=1}^{n} d_x(t)e^{i2\pi kx/n}, \\ \nu_k(t) &= \frac{1}{\sqrt{n}}\sum_{x=1}^{n} n_x(t)e^{i2\pi kx/n}, \end{aligned} \tag{A4}$$

where

$$\begin{aligned} d_x(t) &= \frac{1}{\sqrt{n}}\sum_{k=0}^{n-1} \delta_k(t)e^{-i2\pi kx/n}, \\ n_x(t) &= \frac{1}{\sqrt{n}}\sum_{k=0}^{n-1} \nu_k(t)e^{-i2\pi kx/n}. \end{aligned} \tag{A5}$$

Here, k is the wave number and takes integer values from 0 to $n-1$, while $\delta_k(t)$ and $\nu_k(t)$ are the Fourier coefficients that take complex values.

Substituting (A5) into (A3), we obtain a system of ordinary differential equations for the coefficients δ_k and ν_k as below:

$$\frac{d}{dt}\begin{pmatrix}\delta_k(t)\\ \nu_k(t)\end{pmatrix} = M_k\begin{pmatrix}\delta_k(t)\\ \nu_k(t)\end{pmatrix}, \tag{A6}$$

where

$$M_k = \begin{pmatrix}-a & -b\\ 2\alpha\ \cos(2\pi k/n) & -d\end{pmatrix}. \tag{A7}$$

Setting

$$\begin{pmatrix}\delta_k(t)\\ \nu_k(t)\end{pmatrix} = \begin{pmatrix}\delta_k(0)\\ \nu_k(0)\end{pmatrix}e^{\lambda_k t}, \tag{A8}$$

we find that λ_k is an eigenvalue of M_k and the solution is dominated by the larger eigenvalue of the Jacobian matrix M_k (if both eigenvalues are real). Therefore, whether the components δ_k, ν_k grow or decay is determined by the sign of λ_k, where

$$\lambda_k = \frac{-(a+d)+\sqrt{(a+d)^2-4[ad+2b\alpha\ \cos(2\pi k/n)]}}{2}. \tag{A9}$$

Note that if λ_k is complex, then the real part of λ_k is negative and so the perturbation decays with time. Since $2\pi k/n$ takes equally spaced values in the range $[0, 2\pi)$, when we set

$$\lambda(\theta) = \frac{-(a+d)+\sqrt{(a+d)^2-4(ad+2b\alpha\ \cos\theta)))}}{2},$$

and if $\max\lambda(\theta) < 0$, pattern formation will not occur. In the Collier model (1), λ_k in (A9) takes its largest value at $k = n/2$ and negative values in the long-wavelength region (Fig. S1). As a result, $|\delta_k|$ exponentially grows if k is near $n/2$ and attenuates for values of k in the other region. It corresponds to the salt and pepper pattern and the necessary and sufficient condition for pattern formation is obtained as below:

$$\lambda_{\max} = \frac{-(a+d)+\sqrt{(a+d)^2-4(ad-2b\alpha)}}{2} > 0. \tag{A10}$$

From (A1) and (A2), we have that

$$\beta(N^0)^{h+1} = -(2r+1)N^0 + 2r. \tag{A11}$$

Thus

$$b = \frac{hv[2r-(2r+1)N^0]}{4r^2(1-N^0)^2}, \tag{A12}$$

$$\alpha = (1-N^0)^2 r, \tag{A13}$$

and

$$2b\alpha = hv\left(1-N^0-\frac{N^0}{2r}\right). \tag{A14}$$

Since $ad = v$ and $0 < N^0 < 1$ from (A2), $ad > 2b\alpha$ if $h \leqslant 1$, so that the inequality (A10) does not hold. Hence a necessary condition for (A10) to hold is $h > 1$.

APPENDIX B: DERIVATION OF THE TIME EVOLUTION EQUATION FOR THE POWER SPECTRUM (21)

From Eq. (20), the value of $\delta_k(t+dt)$ is given by

$$\delta_k(t+dt) = \delta_k(t) + \lambda_k\delta_k(t)dt + \sum_{j=1}^{n}\sum_{l=0}^{n-1}\{C^j - I\}_{k+1,l+1}\delta_l(t)dL_t^{p,j}. \tag{B1}$$

The value of the power spectrum $P_k(t+dt) = |\delta_k(t+dt)|^2$ is obtained by multiplying $\delta_k(t+dt)$ in (B1) by its complex conjugate $\overline{\delta}_k(t+dt)$ as below:

$$|\delta_k(t+dt)|^2 = |\delta_k(t)|^2 + \lambda_k|\delta_k(t)|^2dt + \overline{\lambda}_k|\delta_k(t)|^2dt + \sum_{j=1}^{n}\left[\left(\overline{\delta}_k(t)\sum_{l=0}^{n-1}\{C^j - I\}_{k+1,l+1}\delta_l(t) + \delta_k(t)\sum_{l=0}^{n-1}\{\overline{C^j} - I\}_{k+1,l+1}\overline{\delta}_l(t)\right)\right.$$
$$\left. + \left(\sum_{l=0}^{n-1}\{C^j - I\}_{k+1,l+1}\delta_l(t)\right)\left(\sum_{l=0}^{n-1}\{\overline{C^j} - I\}_{k+1,l+1}\overline{\delta}_l(t)\right)\right]dL_t^{p,j} + O(dL^{p,j}\,dt) + O(dt^2). \tag{B2}$$

Here we used the result

$$\left(dL_t^{p,j}\right)\left(dL_t^{p,\xi}\right) = \begin{cases}0 & \text{if } j \neq \xi,\\ dL_t^{p,j} & \text{if } j = \xi.\end{cases} \tag{B3}$$

By denoting $a_k^j = \sum_{l=0}^{n-1}\{C^j\}_{k+1,l+1}\delta_l$, we obtain

$$\sum_{l=0}^{n-1}\left\{C^j - I\right\}_{k+1,l+1}\delta_l(t) = a_k^j(t) - \delta_k(t). \tag{B4}$$

Substituting (B4) into (B2), we obtain (ignoring higher order terms)

$$|\delta_k(t+dt)|^2 = |\delta_k(t)|^2 + 2\,\mathrm{Re}[\lambda_k]|\delta_k(t)|^2 dt + \sum_{j=1}^{n}\left[\left|a_k^j(t)\right|^2 - |\delta_k(t)|^2\right] dL_t^{p,j}$$
$$= |\delta_k(t)|^2 + 2\,\mathrm{Re}[\lambda_k]|\delta_k(t)|^2 dt + \sum_{j=1}^{n}\left[\left|\sum_{l=0}^{n-1}\{C^j\}_{k+1,l+1}\delta_l(t)\right|^2 - |\delta_k(t)|^2\right] dL_t^{p,j}. \tag{B5}$$

The third term on the right-hand side of (B5) is the effect of cell flipping on the power spectrum for the flip position j. Based on the symmetry of the cell position j in the system (5), we assume that the third term on the right-hand side of (B5) can be approximated by replacing the effect of each flip event with $\mathcal{W}_k$, which is the averaged effect for the flip position j as below:

$$\sum_{j=1}^{n}\left[\left|\sum_{l=0}^{n-1}\{C^j\}_{k+1,l+1}\delta_l(t)\right|^2 - |\delta_k(t)|^2\right] dL_t^{p,j} \simeq \sum_{j=1}^{n}\mathcal{W}_k dL_t^{p,j} = \mathcal{W}_k dL_t^{pn}, \tag{B6}$$

where

$$\mathcal{W}_k = \frac{1}{n}\sum_{j=1}^{n}\left[\left|\sum_{l=0}^{n-1}\{C^j\}_{k+1,l+1}\delta_l(t)\right|^2 - |\delta_k(t)|^2\right] = \frac{1}{n}\sum_{j=1}^{n}\left[\left|\sum_{l=0}^{n-1}\{C^j\}_{k+1,l+1}\delta_l(t)\right|^2\right] - |\delta_k(t)|^2. \tag{B7}$$

Here, we used $\sum_{j=1}^{n} dL_t^{p,j} = dL_t^{pn}$ and note that

$$\frac{1}{n}\sum_{j=1}^{n}\left[\left|\sum_{l=0}^{n-1}\{C^j\}_{k+1,l+1}\delta_l(t)\right|^2\right] = \frac{1}{n}\sum_{m=0}^{n-1}\sum_{l=0}^{n-1}\left[\delta_l\overline{\delta_m}\left(\sum_{j=1}^{n}\{C^j\}_{k+1,l+1}\overline{\{C^j\}}_{k+1,m+1}\right)\right]. \tag{B8}$$

From (17), the components of the matrix C^j are given as below:

$$\{C^j\}_{k,l} = \begin{cases} -\frac{4}{n}\sin\frac{\pi(l-1)}{n}\sin\frac{\pi(k-1)}{n}e^{\frac{i\pi(2j-1)(k-l)}{n}} & \text{if } k \neq l, \\ 1 - \frac{4}{n}\sin^2\frac{\pi(k-1)}{n} & \text{if } k = l, \end{cases} \tag{B9}$$

so

$$\sum_{j=1}^{n}\{C^j\}_{k+1,l+1}\overline{\{C^j\}}_{k+1,m+1} = \begin{cases} 0 & \text{if } l \neq m, \\ \frac{16}{n}\sin^2\frac{\pi k}{n}\sin^2\frac{\pi l}{n} & \text{if } l = m \text{ and } k \neq m, \\ n\left(1 - \frac{4}{n}\sin^2\frac{\pi k}{n}\right)^2 & \text{if } k = l = m. \end{cases} \tag{B10}$$

Here we used

$$\sum_{j=1}^{n} e^{i\pi(2j-1)(l-m)/n} = \begin{cases} 0 & \text{if } l \neq m, \\ n & \text{if } l = m. \end{cases} \tag{B11}$$

Therefore, from (B8) and (B10), we obtain

$$\frac{1}{n}\sum_{j=1}^{n}\left[\left|\sum_{l=0}^{n-1}\{C^j\}_{k+1,l+1}\delta_l(t)\right|^2\right] = \frac{1}{n}\sum_{\substack{l=0 \\ l\neq k}}^{n-1}\left[|\delta_l(t)|^2\frac{16}{n}\sin^2\frac{\pi k}{n}\sin^2\frac{\pi l}{n}\right] + |\delta_k(t)|^2\left(1 - \frac{8}{n}\sin^2\frac{\pi k}{n} + \frac{16}{n^2}\sin^4\frac{\pi k}{n}\right)$$
$$= \sum_{l=0}^{n-1}\left[\left(\frac{4}{n}\sin\frac{\pi k}{n}\sin\frac{\pi l}{n}\right)^2|\delta_l(t)|^2\right] + \left(1 - \frac{8}{n}\sin^2\frac{\pi k}{n}\right)|\delta_k(t)|^2. \tag{B12}$$

By replacing the third term on the right-hand side of (B5) by the averaged effect (B6) and substituting (B7) and (B12), we obtain

$$|\delta_k(t+dt)|^2 \simeq |\delta_k(t)|^2 + 2\,\mathrm{Re}[\lambda_k]|\delta_k(t)|^2 dt + \frac{1}{n}\sum_{j=1}^{n}\left[\left|\sum_{l=0}^{n-1}\{C^j\}_{k+1,l+1}\delta_l(t)\right|^2 - |\delta_k(t)|^2\right] dL_t^{pn}$$
$$= |\delta_k(t)|^2 + 2\,\mathrm{Re}[\lambda_k]|\delta_k(t)|^2 dt + \left(\sum_{l=0}^{n-1}\left[\left(\frac{4}{n}\sin\frac{\pi k}{n}\sin\frac{\pi l}{n}\right)^2|\delta_l(t)|^2\right] - \frac{8}{n}\sin^2\frac{\pi k}{n}|\delta_k(t)|^2\right) dL_t^{pn}. \tag{B13}$$

Therefore, the time evolution of the power spectrum can be represented more concisely in the form

$$d\boldsymbol{P} = 2\,\mathrm{Re}[\Lambda]\boldsymbol{P}\,dt + W\boldsymbol{P}\,dL_t^{pn}, \tag{B14}$$

where Λ is given in (15), $\boldsymbol{P} = [|\delta_0(t)|^2, |\delta_1(t)|^2, \ldots, |\delta_k(t)|^2, \ldots, |\delta_{n-1}(t)|^2]^{\mathsf{T}}$, and

$$\{W\}_{l,m} = \begin{cases} -\frac{8}{n}\sin^2\frac{\pi(l-1)}{n} + \left(\frac{4}{n}\sin^2\frac{\pi(l-1)}{n}\right)^2 & (l=m), \\ \left(\frac{4}{n}\sin\frac{\pi(l-1)}{n}\sin\frac{\pi(m-1)}{n}\right)^2 & (\text{otherwise}). \end{cases} \tag{B15}$$

APPENDIX C: DERIVATION OF THE TIME EVOLUTION OF THE POWER SPECTRUM (36)

From Eq. (31), the components of the matrix $\hat{C}^j$ are given as below:

$$\{\hat{C}^j\}_{k,l} = \begin{cases} \sqrt{(n+1)/n} & (\text{if } k=l=1), \\ -\frac{1}{\sqrt{n(n+1)}}\frac{\sin\left(\frac{\pi(l-1)}{n}\right)}{\sin\left(\frac{\pi(k-1)}{n+1}-\frac{\pi(l-1)}{n}\right)}e^{i\pi\left(\frac{(2j-1)(k-1)}{n+1}-\frac{2(j-1)(l-1)}{n}\right)} & (\text{otherwise}). \end{cases} \tag{C1}$$

The power spectrum after proliferation of cell j is obtained from the Fourier coefficient δ_k before proliferation as below:

$$\begin{aligned} |\delta_{k-1}|^2{}^{j}_{\text{after}} &= \left(\sum_{l=1}^{n}\{\hat{C}^j\}_{k,l}\delta_{l-1}\right)\left(\sum_{m=1}^{n}\{\overline{\hat{C}}^j_{k,m}\}\overline{\delta}_{m-1}\right) \\ &= \sum_{m=1}^{n}\sum_{l=1}^{n}[\{\hat{C}^j\}_{k,l}\{\overline{\hat{C}}^j\}_{k,m}\delta_{l-1}\overline{\delta}_{m-1}]. \end{aligned} \tag{C2}$$

As in the cell mixing model, the time evolution of the power spectrum is approximated by replacing the effect of each proliferation event with an average effect. Considering the average effect on the power spectrum, we calculate the average of $|\delta_k|^2{}^{j}_{\text{after}}$ over j:

$$\begin{aligned} \frac{1}{n}\sum_{j=1}^{n}|\delta_{k-1}|^2{}^{j}_{\text{after}} &= \frac{1}{n}\sum_{j=1}^{n}\sum_{m=1}^{n}\sum_{l=1}^{n}[\{\hat{C}^j\}_{k,l}\{\overline{\hat{C}}^j\}_{k,m}\delta_{l-1}\overline{\delta}_{m-1}] \\ &= \frac{1}{n}\sum_{m=1}^{n}\sum_{l=1}^{n}\delta_{l-1}\overline{\delta}_{m-1}\left[\sum_{j=1}^{n}\{\hat{C}^j\}_{k,l}\{\overline{\hat{C}}^j\}_{k,m}\right] \end{aligned} \tag{C3}$$

and

$$\begin{aligned} &\sum_{j=1}^{n}\{\hat{C}^j\}_{k,l}\{\overline{\hat{C}}^j\}_{k,m} \\ &= \begin{cases} 0 & \text{if } l\neq m, \\ \frac{1}{(n+1)}\frac{\sin^2\frac{\pi(l-1)}{n}}{\sin^2\left(\frac{\pi(k-1)}{n+1}-\frac{\pi(l-1)}{n}\right)} & \text{if } l=m \text{ and } l\neq 1, \\ (n+1) & \text{if } k=l=m=1. \end{cases} \end{aligned} \tag{C4}$$

Here we used the fact that

$$\sum_{j=1}^{n}e^{i2\pi(j-1)(l-m)/n} = \begin{cases} 0 & \text{if } l\neq m, \\ n & \text{if } l=m. \end{cases} \tag{C5}$$

Hence

$$\begin{aligned} &\frac{1}{n}\sum_{j=1}^{n}|\delta_{k-1}|^2{}^{j}_{\text{after}} \\ &= \begin{cases} \sum_{l=1}^{n}\frac{1}{n(n+1)}\frac{\sin^2\left(\frac{\pi(l-1)}{n}\right)}{\sin^2\left(\frac{\pi(k-1)}{n+1}-\frac{\pi(l-1)}{n}\right)}|\delta_{l-1}|^2 & \text{if } k\neq 1, \\ \frac{n+1}{n}|\delta_0|^2 + \frac{1}{n(n+1)}\sum_{l=2}^{n}|\delta_{l-1}|^2 & \text{if } k=1. \end{cases} \end{aligned} \tag{C6}$$

Therefore, the effect of a single proliferation event on the power spectrum is represented by the matrix S in (34).

Since the Delta expression D_x are real values, it follows that $P_k = P_{n-k}$. Because of this symmetry, $\boldsymbol{P}_n$ can be represented by the superposition of cosine waves:

$$\boldsymbol{P}_n = \sum_{k=0}^{n-1}e_k\boldsymbol{z}_k^n, \tag{C7}$$

$$\boldsymbol{z}_k^n = \left(1, \cos\frac{2\pi k}{n}, \cos\frac{4\pi k}{n}, \ldots, \cos\frac{2(n-1)\pi k}{n}\right)^{\mathsf{T}}. \tag{C8}$$

Here, e_k are the coefficients of the cosine waves, and z_k^n is obtained by discrete and equal sampling of $\cos 2\pi kx$. From the orthogonality of the trigonometric function, we obtain

$$\boldsymbol{e} = Z\boldsymbol{P}_n, \tag{C9}$$

where $\boldsymbol{e} = (e_0, e_1, \ldots, e_{n-1})^{\mathsf{T}}$ and Z is a square $n\times n$ matrix such that

$$\{Z\}_{l,m} = \cos\frac{2\pi(l-1)(m-1)}{n}. \tag{C10}$$

From the symmetry of $\boldsymbol{P}_n$, we can also obtain e_k as a discrete Fourier transform of $\boldsymbol{P}_n$. As the discrete Fourier transform of the power spectrum is the autocorrelation function (from the Wiener-Khinchin theorem), e_k corresponds to the averaged autocorrelation function of D_x.

$S\boldsymbol{P}_n$ is also represented by the superposition of cosine waves with different coefficients $\hat{e}_k$:

$$S\boldsymbol{P}_n = \sum_{k=0}^{n}\hat{e}_k\boldsymbol{z}_k^{n+1}. \tag{C11}$$

Therefore, the power spectra $\boldsymbol{P}_n$ and $S\boldsymbol{P}_n$ can be regarded as the sampled values of the function $P(\theta)$ and $P(\theta)_{\text{after}}$, respectively:

$$P(\theta) = \sum_{k=0}^{n-1}e_k\cos kx, \tag{C12}$$

$$P(\theta)_{\text{after}} = \sum_{k=0}^{n}\hat{e}_k\cos kx. \tag{C13}$$

Hence, the matrix S can be regarded as a map that transforms the coefficients of superposition e_k to $\hat{e}_k$.

The vector $2\,\text{Re}[\Lambda]\boldsymbol{P}_n$ is also regarded as the sampled values of the function $2\lambda(\theta)P(\theta)$, where

$$\lambda(\theta) = \text{Re}\left[\frac{-(a+d)+\sqrt{(a+d)^2-4(ad+2b\alpha\cos\theta)}}{2}\right]. \tag{C14}$$

Therefore, the stability of the power spectrum vector $\boldsymbol{P}_n$ can be examined by approximating S with a square matrix Σ such that $\Sigma\boldsymbol{P}_n$ shares the same coefficients of the superposition of the cosine wave with $S\boldsymbol{P}_n$.

We write

$$S = \frac{1}{n}\hat{Z}QZ, \tag{C15}$$

where $\hat{Z}$ is a square $(n+1)\times(n+1)$ matrix and Q is an $(n+1)\times n$ matrix whose components are, respectively,

$$\{\hat{Z}\}_{l,m} = \cos\frac{2\pi(l-1)(m-1)}{n+1} \tag{C16}$$

and

$$\{Q\}_{l,m} = \begin{cases} (n+2-l)/(n+1) & (\text{if } l=m), \\ (l-1)/(n+1) & (\text{if } l+1=m \text{ and } l\geqslant 2), \\ 1/(n+1) & (\text{if } l=n \text{ and } m=1), \\ 0 & (\text{otherwise}). \end{cases} \tag{C17}$$

Therefore, the coefficients $\hat{e}_k$ are determined by e_k as follows:

$$\begin{aligned} \hat{e}_0 &= e_0, \\ \hat{e}_k &= \frac{n+1-k}{n+1}e_k + \frac{k}{n+1}e_{k-1} \quad (1\leqslant k\leqslant n-1), \\ \hat{e}_n &= \frac{n}{n+1}e_{n-1} + \frac{1}{n+1}e_0. \end{aligned} \tag{C18}$$

This relationship is derived from the formulas in Supplemental text B [28].

When n is even, we define an $n\times n$ square matrix $\hat{Q}$ by removing the $(n/2+1)$th row of the matrix Q and then define an $n\times n$ square matrix Σ such that

$$\Sigma = Z\hat{Q}Z. \tag{C19}$$

Here,

$$\begin{aligned} \{\Sigma\}_{l,m} = \frac{2}{n}\sum_{k=2}^{n/2}\cos\frac{2\pi(m-1)(k-1)}{n}\left[\frac{k-1}{n+1}\cos\frac{2\pi(l-1)(k-2)}{n} + \left(1-\frac{k-1}{n+1}\right)\cos\frac{2\pi(l-1)(k-1)}{n}\right] \\ + \frac{1}{n}\left[1+(-1)^{m+l-2}\left(1-\frac{n}{n+1}\sin^2\frac{\pi(l-1)}{n}\right)\right]. \end{aligned} \tag{C20}$$

The n-dimensional vector $\Sigma\boldsymbol{P}_n$ is represented as the superposition of the cosine waves:

$$\Sigma\boldsymbol{P}_n = \sum_{k=0}^{n/2}\hat{e}_k\boldsymbol{z}_k^n + \sum_{k=n/2+1}^{n-1}\hat{e}_{k+1}\boldsymbol{z}_k^n. \tag{C21}$$

Since $z_k^n = z_{n-k}^n$ holds and n is even, Eq. (C11) can be simplified:

$$S\boldsymbol{P}_n = \sum_{k=0}^{n/2}\tilde{e}_k\boldsymbol{z}_k^{n+1}, \tag{C22}$$

$$\tilde{e}_k = \begin{cases} \hat{e}_k & (\text{if } k=0), \\ \hat{e}_k + \hat{e}_{n-k} & (\text{otherwise}). \end{cases} \tag{C23}$$

Equation (C21) can also be simplified:

$$\Sigma\boldsymbol{P}_n = \left(\sum_{k=0}^{n/2-1}\tilde{e}_k\boldsymbol{z}_k^n\right) + \hat{e}_{n/2}\,\boldsymbol{z}_{n/2}^n. \tag{C24}$$

When n is odd, we define an $n\times n$ square matrix $\hat{Q}$ by removing the $[(n+3)/2]$th row of the matrix Q and define an $n\times n$ square matrix Σ such that

$$\Sigma = Z\hat{Q}Z. \tag{C25}$$

Here,

$$\{\Sigma\}_{l,m} = \frac{2}{n}\sum_{k=2}^{(n+1)/2}\cos\frac{2\pi(m-1)(k-1)}{n}\left[\frac{k-1}{n+1}\cos\frac{2\pi(l-1)(k-2)}{n} + \left(1-\frac{k-1}{n+1}\right)\cos\frac{2\pi(l-1)(k-1)}{n}\right] + \frac{1}{n}. \tag{C26}$$

The n-dimensional vector $\Sigma\boldsymbol{P}_n$ is represented as the superposition of the cosine waves:

$$\Sigma\boldsymbol{P}_n = \sum_{k=0}^{(n-1)/2}\hat{e}_k\boldsymbol{z}_k^n + \sum_{k=(n+1)/2}^{n-1}\hat{e}_{k+1}\boldsymbol{z}_k^n. \tag{C27}$$

Since n is odd, Eq. (C11) can be simplified:

$$S\boldsymbol{P}_n = \sum_{k=0}^{(n+1)/2}\tilde{e}_k\boldsymbol{z}_k^{n+1}, \tag{C28}$$

$$\tilde{e}_k = \begin{cases} \hat{e}_k & [\text{if } k=0 \text{ or } (n+1)/2], \\ \hat{e}_k + \hat{e}_{n-k} & (\text{otherwise}). \end{cases} \tag{C29}$$

Equation (C27) can also be simplified:

$$\Sigma\boldsymbol{P}_n = \sum_{k=0}^{(n-1)/2}\tilde{e}_k\boldsymbol{z}_k^n. \tag{C30}$$

Comparing (C24) with (C22) and (C30) with (C28), $\Sigma\boldsymbol{P}_n$ and $S\boldsymbol{P}_n$ can share the coefficients of the superposition of the cosine wave except for that of the shortest wavelength ($\tilde{e}_{n/2}$ when n is even and $\tilde{e}_{(n+1)/2}$ when n is odd).

The shortest wavelength component of the superposition $\tilde{e}_{n/2}$ or $\tilde{e}_{(n+1)/2}$ corresponds to the long-range correlation of the Delta expression pattern $\boldsymbol{D}_n$. Since the Delta-Notch interaction and cell proliferation locally affect the pattern, we expect the

long-range correlation to be small. Thus the contribution of the shortest wavelength component of the cosine wave superposition alone to the spectral structure of the power spectrum would be small when n is sufficiently large. Therefore, Σ is a square matrix that approximates S, in the sense that it preserves the spectral structure of the power spectrum. Based on this assumption, we can analyze Eq. (34) in the same way as in the cell mixing model by replacing S with Σ and find that it gives results that agree with the numerical results of the cell proliferation model (7) [Figs. 4(d) and 4(f)].

[1] O. L. Mohr, Genetics **4**, 275 (1919).
[2] J. R. Collier, N. A. M. Monk, P. K. Maini, and J. H. Lewis, J. Theor. Biol. **183**, 429 (1996).
[3] D. Sprinzak, A. Lakhanpal, L. LeBon, L. A. Santat, M. E. Fontes, G. A. Anderson, J. Garcia-Ojalvo, and M. B. Elowitz, Nature (London) **465**, 86 (2010).
[4] F. Vilas-Boas, R. Fior, J. R. Swedlow, K. G. Storey, and D. Henrique, BMC Biol. **9**, 58 (2011).
[5] O. Shaya and D. Sprinzak, Curr. Opin. Genet. Dev. **21**, 732 (2011).
[6] M. Matsuda, M. Koga, E. Nishida, and M. Ebisuya, Sci. Signal **5**, ra31 (2012).
[7] K. Uriu and L. G. Morelli, Dev. Growth Differ. **59**, 351 (2017).
[8] A. M. Herman, A. M. Rhyner, W. P. Devine, S. P. Marrelli, B. G. Bruneau, and J. D. Wythe, Biol. Open **7**, bio.026799 (2018).
[9] M. E. Pitulescu, I. Schmidt, B. D. Giaimo, T. Antoine, F. Berkenfeld, F. Ferrante, H. Park, M. Ehling, D. Biljes, S. F. Rocha, U. H. Langen, M. Stehling, T. Nagasawa, N. Ferrara, T. Borggrefe, and R. H. Adams, Nat. Cell Biol. **19**, 915 (2017).
[10] M. Eddison, I. L. Roux, and J. Lewis, Proc. Natl. Acad. Sci. USA **97**, 11692 (2000).
[11] E. Chrysostomou, J. E. Gale, and N. Daudet, Development **139**, 3764 (2012).
[12] J. Neves, G. Abelló, J. Petrovic, and F. Giraldez, Dev. Growth Differ. **55**, 96 (2013).
[13] S. Claxton and M. Fruttiger, Gene Expr. Patterns **5**, 123 (2004).
[14] J. J. Hofmann and M. L. Iruela-Arispe, Gene Expr. Patterns **7**, 461 (2006).
[15] S. S. Hasan, R. Tsaryk, M. Lange, L. Wisniewski, J. C. Moore, N. D. Lawson, K. Wojciechowska, H. Schnittler, and A. F. Siekmann, Nat. Cell Biol. **19**, 928 (2017).
[16] M. Cohen, B. Baum, and M. Miodownik, J. R. Soc. Interface **8**, 787 (2010).
[17] M. B. Elowitz, A. J. Levine, E. D. Siggia, and P. S. Swain, Science **297**, 1183 (2002).
[18] D. A. Charlebois, N. Abdennur, and M. Kaern, Phys. Rev. Lett. **107**, 218101 (2011).
[19] T. Rudge and K. Burrage, Bull. Math. Biol. **70**, 971 (2008).
[20] A. I. Reppas, G. Lolas, A. Deutsch, and H. Hatzikirou, ACM Trans. Model. Comput. Simul. **26**, 1 (2016).
[21] M. Noguchi, K. Sumiyama, and M. Morimoto, Cell Rep. **13**, 2679 (2015).
[22] P.-N. Tsao, C. Matsuoka, S.-C. Wei, A. Sato, S. Sato, K. Hasegawa, H.-k. Chen, T.-Y. Ling, M. Mori, W. V. Cardoso, and M. Morimoto, Proc. Natl. Acad. Sci. USA **113**, 8242 (2016).
[23] S. Arima, K. Nishiyama, T. Ko, Y. Arima, Y. Hakozaki, K. Sugihara, H. Koseki, Y. Uchijima, Y. Kurihara, and H. Kurihara, Development **138**, 4763 (2011).
[24] W. Luo, I. Garcia-Gonzalez, M. Fernández-Chacón, V. Casquero-Garcia, M. S. Sanchez-Muñoz, S. Mühleder, L. Garcia-Ortega, J. Andrade, M. Potente, and R. Benedito, Nature (London) **589**, 437 (2020).
[25] R. Riahi, J. Sun, S. Wang, M. Long, D. D. Zhang, and P. K. Wong, Nat. Commun. **6**, 6556 (2015).
[26] D. P. J. Germano and J. M. Osborne, J. Theor. Biol. **514**, 110535 (2021).
[27] D. Stepanova, H. M. Byrne, P. K. Maini, and T. Alarcón, PLoS Comput. Biol. **17**, e1008055 (2021).
[28] See Supplemental Material at http://link.aps.org/supplemental/10.1103/PhysRevE.107.064404 for additional information and figures.
[29] P. Formosa-Jordan, Pattern formation through lateral inhibition mediated by Notch signaling, Ph.D. thesis, Universitat de Barcelona, 2013.
[30] H. X. Chao, R. I. Fakhreddin, H. K. Shimerov, K. M. Kedziora, R. J. Kumar, J. Perez, J. C. Limas, G. D. Grant, J. G. Cook, G. P. Gupta, and J. E. Purvis, Mol. Syst. Biol. **15**, e8604 (2019).
[31] P. Formosa-Jordan and M. Ibañes, PLoS One **9**, e95744 (2014).
[32] S. Pontes-Quero, M. Fernández-Chacón, W. Luo, F. F. Lunella, V. Casquero-Garcia, I. Garcia-Gonzalez, A. Hermoso, S. F. Rocha, M. Bansal, and R. Benedito, Nat. Commun. **10**, 2016 (2019).
[33] C. Xu, S. S. Hasan, I. Schmidt, S. F. Rocha, M. E. Pitulescu, J. Bussmann, D. Meyen, E. Raz, R. H. Adams, and A. F. Siekmann, Nat. Commun. **5**, 5758 (2014).
[34] B. Weijts, E. Gutierrez, S. K. Saikin, A. J. Ablooglu, D. Traver, A. Groisman, and E. Tkachenko, Nat. Commun. **9**, 5314 (2018).
[35] M. K. Jolly, M. Boareto, M. Lu, J. N. Onuchic, C. Clementi, and E. Ben-Jacob, New J. Phys. **17**, 055021 (2015).
[36] K. Uriu, S. Ares, A. C. Oates, and L. G. Morelli, Phys. Rev. E **87**, 032911 (2013).
[37] T. Abe, H. Kiyonari, G. Shioi, K. Inoue, K. Nakao, S. Aizawa, and T. Fujimori, genesis **49**, 579 (2011).
[38] J. M. Ogilvie, J. D. Speck, J. M. Lett, and T. T. Fleming, J. Neurosci. Methods **87**, 57 (1999).
[39] J. Schindelin, I. Arganda-Carreras, E. Frise, V. Kaynig, M. Longair, T. Pietzsch, S. Preibisch, C. Rueden, S. Saalfeld, and B. Schmid, Nat. Methods **9**, 676 (2012).
[40] J. Tinevez, N. Perry, J. Schindelin, G. M. Hoopes, G. D. Reynolds, E. Laplantine, S. Y. Bednarek, S. L. Shorte, and K. W. Eliceiri, Methods **115**, 80 (2017).
[41] R. Jentzsch, J. R. Angew. Math. **1912**, 235 (1912).
[42] X. Wang and D.-Y. Zheng, J. Math. Anal. Appl. **335**, 1020 (2007).
[43] W. Ejsmont and F. Lehner, J. Comb. Theory Ser. A **177**, 105324 (2021).